Publ. Astron. Soc. Japan (2018) 70 (5), 93 (1–8)
doi: 10.1093/pasj/psy089
Advance Access Publication Date: 2018 August 30

A 100 pc-scale fast and dense outflow in the narrow-line Seyfert 1 galaxy IRAS 04576+0912

Toshihiro Kawaguchi,[1,*] Shinobu Ozaki,[2] Hajime Sugai,[3] Kazuya Matsubayashi,[4] Takashi Hattori,[5] Atsushi Shimono,[3] Kentaro Aoki,[5] Yutaka Hayano,[2] Yosuke Minowa,[5] Kazuma Mitsuda,[6] and Yasuhito Hashiba[7]

[1]Department of Economics, Management and Information Science, Onomichi City University, Hisayamada 1600-2, Onomichi, Hiroshima 722-8506, Japan
[2]National Astronomical Observatory of Japan, 2-21-1 Osawa, Mitaka, Tokyo 181-8588, Japan
[3]Kavli IPMU (WPI), The University of Tokyo, 5-1-5 Kashiwanoha, Kashiwa, Chiba 277-8583, Japan
[4]Okayama Astrophysical Observatory, Honjo 3037-5, Kamogata, Okayama 719-0232, Japan
[5]Subaru Telescope, National Astronomical Observatory of Japan, 650 North A'hoku Place, Hilo, HI 96720, USA
[6]Astronomical Institute, Tohoku University, 6-3 Aramaki, Aoba-ku, Sendai, Miyagi 980-8578, Japan
[7]Institute of Astronomy, The University of Tokyo, 2-21-1 Osawa, Mitaka, Tokyo 181-0015, Japan

*E-mail: kawaguchi@onomichi-u.ac.jp

Received 2018 March 3; Accepted 2018 July 17

Abstract

We report the initial results of an adaptive-optics-assisted, optical integral-field-unit observation of IRAS 04576+0912, the nearest ($z = 0.039$) active galactic nucleus with a prominent blueshift/tail in [O III] emission from a sample of such objects that we have collected from the literature. We aim at addressing the putative quasar-mode feedback process with Subaru/Kyoto 3D II+AO188. The optical waveband (6400–7500 Å) enables us to measure the gas density via the [S II] doublets, in contrast to earlier near-IR studies. Since the fast [O III] outflow happens only around rapidly growing central black holes, this object is suitable for investigating the black hole–galaxy coevolution. The obtained data cube exhibits a blue tail in the [S II] emission at many lenslets. By fitting the spectrum with the high excess flux at the [S II] bluetail, we find a fast ($\sim$860 km s^{-1}), dense ($>$3000 cm^{-3}), wide-angle, and offset outflow in central 100 pc scales. Although the large opening angle and the high gas outflow-to-accretion ratio may favor the feedback hypothesis, the inferred kinetic power injection rate of this ionized gas outflow seems insufficient to influence the whole host galaxy. A conventional assumption of a low density must have overestimated the feedback process.

Key words: galaxies: active — galaxies: individual (IRAS 04576+0912) — galaxies: kinematics and dynamics — galaxies: nuclei — galaxies: Seyfert

1 Introduction

Various investigations on the evolution of galaxies and massive black holes (BHs) indicate a strong outflow, driven by the radiation from the accretion disk of active galactic nuclei (AGNs) (e.g., Silk & Rees 1998). It is required to self-regulate star formation of host galaxies and to hamper the

production of too-massive galaxies ("quasar-mode feedback"; e.g., Schawinski et al. 2007). There is much evidence for outflows from AGNs, observed as C IV bluetail, [O III] blueshift, broad and narrow absorption lines (BALs and NALs), X-ray and many other lines (e.g., Zamanov et al. 2002; Sulentic et al. 2007). Winds from quasars may have played a major role in the BH–galaxy coevolution (e.g., Wyithe & Loeb 2003; Di Matteo et al. 2005). However, a similar number of works indicate that the AGN feedback is not efficient enough (Gabor & Bournaud 2014; Balmaverde et al. 2016; Carniani et al. 2016; Villar-Martín et al. 2016).

Due to the lack of density indicators or sufficient spatial resolution in earlier observations, basic questions on the putative quasar-mode feedback, such as if there really is a quasar-mode feedback, if it is powerful enough to quench star formation, or if every AGN launches the feedback, are still unclear.

We carried out adaptive-optics (AO) assisted, optical integral-field-unit (IFU) observations for nearby AGNs that are plausible candidates in the act of feedback. Our targets were selected from objects that evidently show blueshifted components in [O III] emission in conventional long-slit spectroscopic data.

The optical wave-band we chose (6400–7500 Å) enabled us to measure the gas density via the flux ratio of the [S II]$\lambda\lambda$6716, 6731Å doublet emission lines (Osterbrock & Ferland 2006). AO-IFUs other than Kyoto 3D II work only in the near-IR band, and hence previous AO-IFU studies assumed the density (e.g., Storchi-Bergmann et al. 2009; Mazzalay et al. 2013), resulting in large uncertainties in the mass outflow rate and the kinetic power etc. of the feedback process. We used Kyoto 3D II with AO188 mounted on the Subaru telescope (Sugai et al. 2010; Matsubayashi et al. 2016). Long-slit spectroscopic data for AGN outflows (e.g., broad wings of emission lines, BALs and NALs) have uncertainties in the geometry and the covering factor, and thus to what degree the outflow influences the interstellar medium (ISM) is unclear. Previous optical IFU observations were not implemented with AO (e.g., Barbosa et al. 2009; Cresci et al. 2015; Lena et al. 2015). The AO assistance is critical for both mapping the outflow with a high spatial sampling (Husemann et al. 2016) and substantial reduction of the major noise source (i.e., broad lines and continuum emission).

In this Letter we report the initial results of our observation for the nearest AGN with prominent [O III] blueshift from a sample of such objects that we collected from the literature. In the next section we briefly describe the selection of our target. Then, observational setups and data reduction are briefly summarized. In section 4 we present the results on the 100 pc-scale fast and dense outflow. Finally, we summarize this study with some discussion in section 5. We adopt the standard ΛCDM cosmology, with $\Omega_\Lambda = 0.714$, $\Omega_M = 0.286$, and $H_0 = 69.6\,\mathrm{km\,s^{-1}\,Mpc^{-1}}$.

2 Target selection

We regard that targets selected from [O III] blueshifting samples are desirable to examine the putative AGN feedback process. This selection ensures that the outflow takes place in the narrow-line region (NLR), overflowing beyond the gravitational potential well of the central BH (~1 pc for a $10^7 M_\odot$ BH). It is uncertain whether outflow in the broad line region (at ~0.01 pc from the center; observed in C IV, X-ray, or BALs) overflows to the galactic scale (~kpc) or is to fall back again.

Our targets are narrow-line Seyfert 1 galaxies (NLS1s), harboring rapidly growing massive BHs (Kawaguchi 2003; Kawaguchi et al. 2004). The [O III] blueshift (with velocity up to $\sim 1000\,\mathrm{km\,s^{-1}}$) occurs only at the phase with high accretion rates onto central BHs (namely, mostly in NLS1s; Marziani et al. 2003; Aoki et al. 2005; Boroson 2005; Komossa et al. 2008). If the AGN feedback process is really efficient, we will then unveil the BH–galaxy coevolution in the early stage of BH growth. The outflow velocity depends on neither the radio power nor radio loudness (Aoki et al. 2005), indicating that the outflow is not powered by small-scale jets.

AGNs with prominent blueshifts in [O III] emission lines were summarized by Aoki, Kawaguchi, and Ohta (2005) and Komossa et al. (2008). To ensure the highest spatial resolution in physical scale, we chose the nearest one among the objects with measured/expected NLR size larger than 1″ in the literature. The nearest object, IRAS 04576+0912 at a redshift z of ~0.039 (subsection 4.4), is an SBa galaxy (Ohta et al. 2007). The field of view (FoV) and the spatial sampling of Kyoto 3D II (3.″1 × 2.″4 and 0.″084) correspond to 2.4 × 1.9 kpc and 65 pc, respectively. Its optical spectrum (Véron-Cetty et al. 2001) shows blueshift in the [O III]$\lambda\lambda$4959, 5007 Å and [N II]λ6584 Å emission lines, by ~300 $\mathrm{km\,s^{-1}}$ (Aoki et al. 2005) from the velocity that matches with the Balmer lines.

The FWHMs of Hα and Hβ emission lines are 1100 $\mathrm{km\,s^{-1}}$ and 1210–1220 $\mathrm{km\,s^{-1}}$, respectively (Véron-Cetty et al. 2001). The estimated BH mass, the bolometric luminosity L_{bol}, and the Eddington ratio are $10^{6.6} M_\odot$, $6.2 \times 10^{44}\,\mathrm{erg\,s^{-1}}$, and 1.15, respectively (Aoki et al. 2005). In a diagram of the BH mass versus the optical luminosity (Kawaguchi 2003), IRAS 04576 is a typical NLS1 and its accretion rate onto the central BH is estimated to be $\sim 0.8\,M_\odot\,\mathrm{yr^{-1}}$.

3 Observation and data reduction

On the night of 2015 September 24 we observed IRAS 04576 and the spectrophotometric standard star (BD +21 607) with Subaru/Kyoto 3D II+AO188 in laser guide star (LGS) mode. Unfortunately, we could use only a half of the FoV due to a temporal detector problem.

We took seven frames, with 1200 s exposure time for each frame. We used the nearby star, 17″ from the center to the NE with $V \sim 15.4$ mag, as the tip–tilt guide star.

During the exposures, the image size (FWHM) of the guide star was about 0.″35–0.″45. The spectral resolution was $R \sim 1200$, and the wavelength coverage 6400–7500 Å.

Data reduction was carried out using custom-made IRAF scripts (Sugai et al. 2010) adapted for the newly installed deep depletion CCD (Mitsuda et al. 2016). The reduction process included bias subtraction, spectrum extraction, and flat fielding. Cosmic rays were removed using L.A.Cosmic (van Dokkum 2001). After wavelength calibration, sky subtraction was performed referring to the sky aperture spectra. Kyoto 3D II simultaneously obtains the spectra of the object and the sky ∼29″ away from the object field. Flux was calibrated using the standard star. Atmospheric absorption features were corrected using the normalized spectrum of the standard star because it is an early-type (F2) star. After converting to the heliocentric velocity, the seven frames were combined. Then, spectral fitting throughout this study was carried out with our own Python code.

4 Line fitting and the results

Before fitting the narrow emission lines, we fixed the two issues that affect their measurements, as described in the next subsection.

4.1 Laser-induced sky emission and broad emission line

The LGS laser excites atmospheric molecules, enhancing their sky emissions via Raman scattering (Vogt et al. 2017). The enhancement is weaker at the science FoV than the sky field, since the secondary mirror tends to hide the former from the scattered light. As a result of sky subtraction, an artificial "absorption" line, at ∼6827 Å (between the Hα and [N II] λ6583 Å lines) due to N_2 molecules in our case, appears in each science spectrum. We fitted the sky spectrum with a Gaussian, and determined the wavelength and the width.

A Fabry–Pérot, narrowband engineering observation in 2015 February showed that the "absorption" depth is constant for the whole science FoV. By fitting the spectra at the north-east and the west ends, showing the clearest "absorption" (with a negative flux density at the corresponding wavelengths), we derived the mean depth of the "absorption," and used it for all the analysis hereafter.

Next, we fixed the shape of the broad Hα emission line. Since the intrinsic size of the broad line region is about 0.01 pc ($\ll$ the angular size of one lenslet) and the apparent spatial extent is due to the point-spread function (PSF) smearing, the line profile should be common among lenslets. We examined which function, among single Gaussian, double Gaussian, and single Lorentzian, could successfully fit the broad line simultaneously in different spatial regions (the four regions in the middle left panel of figure 1). We found the double Gaussian to be most successful. Of the two components of the double Gaussian, the narrower and higher one has the central wavelength and the FWHM of 6817.96 Å and 1306 km s^{-1}, while the broader and lower one has 6814.41 Å and 2579 km s^{-1}, respectively. The peak ratio of the second over the first of 0.49 was fixed for the entire FoV.

4.2 Fit with single narrow-line component

For the 615 lenslets with large enough flux at line-free wavelengths compared with the sky spectrum, we fitted each spectrum at 6600–7200 Å by a combination of a linear continuum, a broad Hα emission line (subsection 4.1) and a single Gaussian velocity component of narrow emission lines with a common line width composed of Hα, [N II]$\lambda\lambda$6548, 6583 Å, and [S II]$\lambda\lambda$6716, 6731 Å. The line ratio of [N II] was fixed so that the 6548 Å/6583 Å flux ratio was 0.34. In figure 1, maps of various line flux, flux ratio, and velocity are shown.

The flux map of the broad Hα line represents the PSF during our observation, and turns out to have a round shape (top left in figure 1). By fitting the map, we obtained the central position and the radial profile, which is well described by a Moffat profile with an FWHM of 0.″37. The PSF FWHM is similar to the image size of the guide star. These indicate successful fitting. The central position indicates the position of the BH.

The [N II]λ6583 Å flux map (upper right) shows an elongation toward the west from the central BH. The maps for the velocity of the narrow emission lines (middle left) and the [N II]/Hα flux ratio (middle right) are also asymmetric in kpc scales. The overall velocity map shows blueshifts on the west and redshifts on the east sides of the BH, indicating galactic rotation with an axis inclined to the north direction. Alternatively, the velocity gradient may imply a double-sided outflowing NLR. Careful decomposition into galactic rotation and NLR kinematics will be needed.

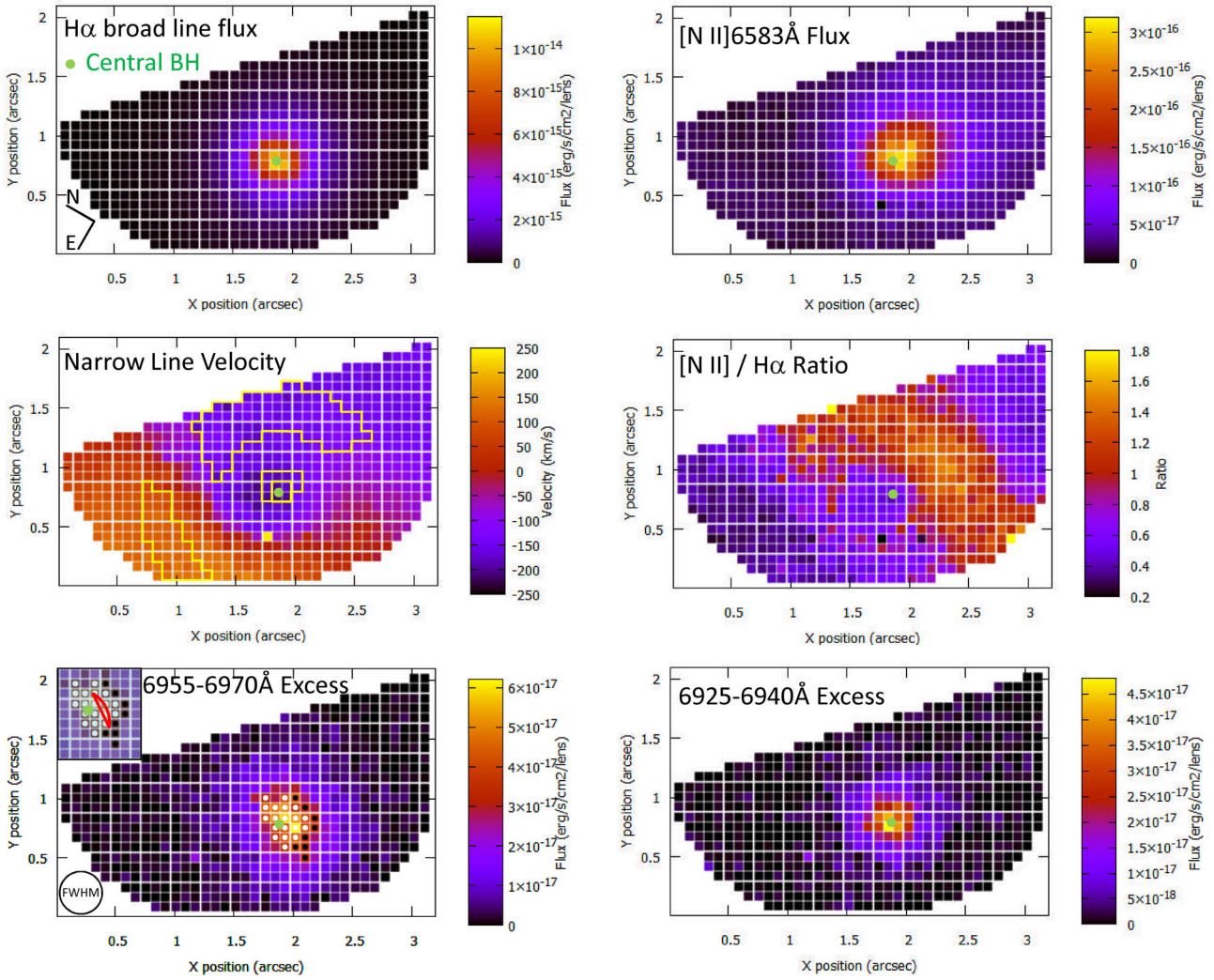

Fig. 1. Maps obtained through the fitting with a single component for narrow emission lines: Hα broad emission flux (top left), [N II] 6583 Å narrow emission flux (top right), velocity of narrow emission lines (middle left, with four yellow regions used for determining the broad line shape; subsection 4.1), the line ratio of [N II] 6583 Å over Hα narrow emission (middle right), excess flux integrated over 6955–6970 Å (bottom left), and that at 6925–6940 Å (bottom right). The horizontal range of 3.″1 corresponds to 2.4 kpc. The circle in the bottom left panel has the diameter of the PSF FWHM, 0.″37 (290 pc), and the inset shows a possible intrinsic structure for the outflowing region. When drawing the velocity map, a systemic velocity was chosen at z of 0.0388 (subsection 4.4).

The [N II]/Hα flux ratio is larger than ∼1.0 at the west of the nucleus, strongly suggesting an AGN origin for the ionization (e.g., Kauffmann et al. 2003). Around the nucleus and ∼1″ to the west, the ratio is relatively lower, but still larger than the border value between AGN and star-formation origins (∼0.5). At 1″–1.″5 northeast of the nucleus, the ratio is even smaller, down to ∼0.3, indicating that there is a star-forming region.

4.3 Outflowing region

When fitting the 615 spectra, it turned out that many lenslets showed a blue tail in the [S II] emission lines (figure 2), indicating an outflowing component of [S II] emission.

To identify the outflowing region, we calculated the excess flux of the observed data over the model (subsection 4.2) at 6955–6970 Å. The bottom left panel in figure 1 shows the excess flux map, where we overdraw 27 (white and black) circles if the excess flux is larger than the half of the maximum excess flux (i.e., larger than 3.1×10^{-17} erg s^{-1} cm^{-2} lens^{-1}). The black circles show the eight lenslets with broad line flux smaller than a certain threshold. We found that the distribution of the white and black circles is not located symmetrically around the central BH: it is mainly distributed at the southwest of the BH. The

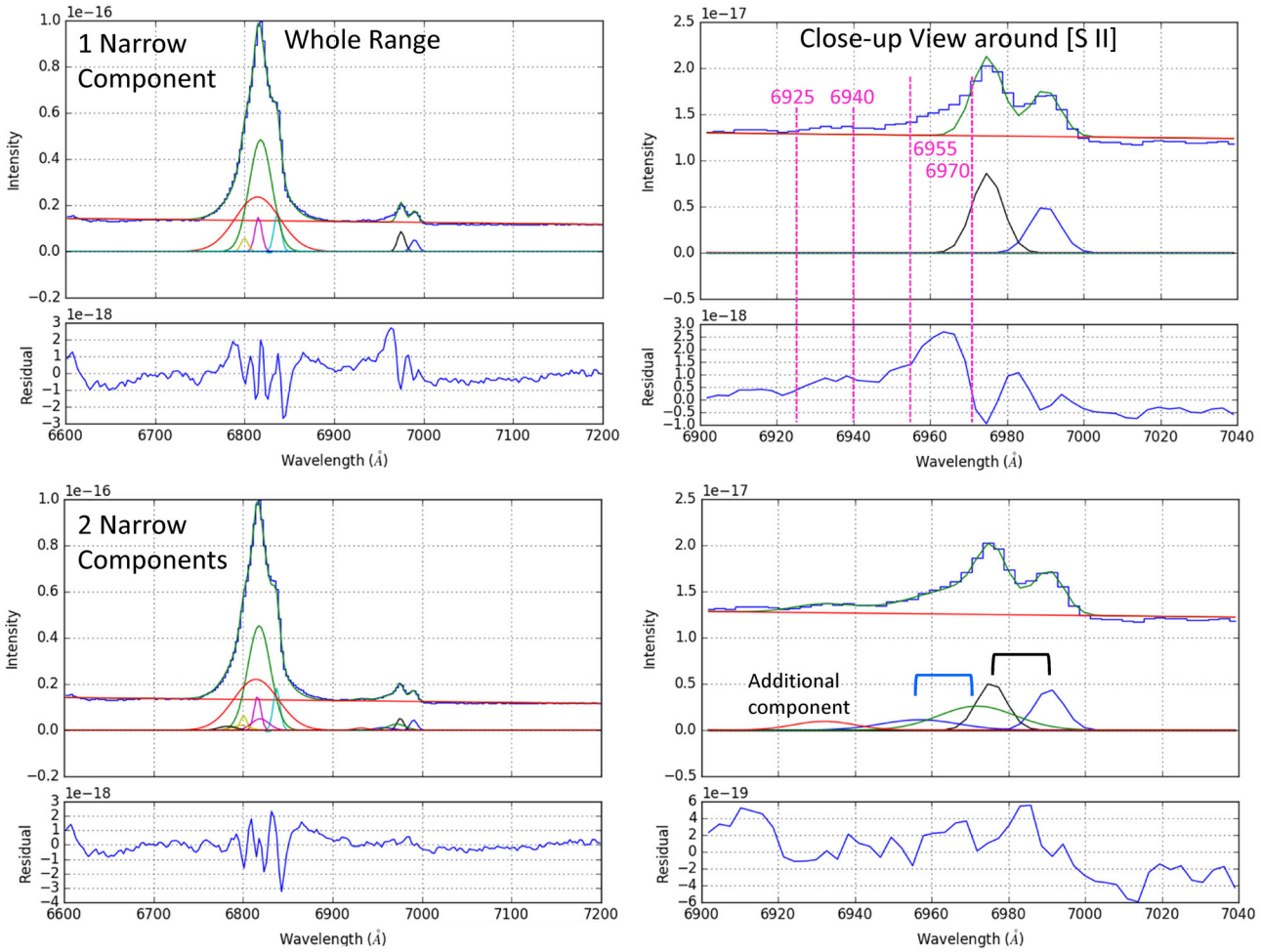

Fig. 2. Spectral fitting for the mean spectrum of the large 6955–6970 Å excess region. The left panels exhibit the whole wavelength range, whereas the right panels show close-up views around the [S II] emission. The upper panels present the result with a single narrow component, while the lower panels were obtained with two narrow components. The vertical dotted lines indicate the two wavelength ranges for the excess flux maps (bottom panels in figure 1).

fact that the outflowing region is offset from the center implies that we are not observing the outflow from the pole-on view.

Moreover, the area with excess flux larger than half of its peak looks elongated, and the elongation is nearly perpendicular to the radial direction from the center. The width is comparable to the PSF FWHM, while the length is about 1.4 times the FWHM. Taking account of image smearing by the PSF, the distribution indicates that the outflowing region is intrinsically narrow (with a length of $\sqrt{1.4^2 - 1^2} \approx 1$ times the FWHM; see the inset of the bottom left panel). The excess flux region offsets from the BH by $\sim$0.″15 ($\sim$120 pc projected distance), implying a short-duration (rather than a continuous) outflow. From the estimated length (1$\times$FWHM) and the offset, we estimate the half-opening angle to be 50° [arctan{(0.″37/2)/0.″15}]. The inferred angle indicates that the outflow is not jet-like (nor spherical). Since a narrow jet-like geometry would have difficulty pushing out or disturbing the ISM of its host galaxy in a large volume, the wide angle estimated above is likely in favor of the AGN feedback hypothesis.

There is a small bump in the spectrum at around 6930 Å (figure 2). To investigate its origin, we show the excess flux map at 6925–6940 Å as well (bottom right panel). The distribution turns out to be similar to that of the broad Hα emission. Namely, this spectral feature is not associated with the region responsible for the [S II] blue tail. Instead, this bump seems to be due to either [S II] line(s) emitted by another outflowing component with a higher velocity near the BH, highly redshifting Hα emission from a blob in the broad line region, or something else (e.g., He Iλ6678 Å). The flux of this bump is consistent with Case B, He Iλ6678 Å recombination at the broad-line region having solar abundance, a temperature of 10^4 K, and an electron density of

Table 1. Fit with two narrow components.

Brighter component	
[S II]λ6731 central wavelength [Å]	6990.63 ± 0.10
FWHM [km s^{-1}]	392.3 ± 14.4
Flux density (6716 Å)*	5.16 ± 0.82
Flux density (6731 Å)*	4.43 ± 0.60
Flux ratio (6716/6731)	1.17 ± 0.24
Gas density [cm^{-3}]	∼300 (20–800)
Blueshifted component	
[S II]λ6731 central wavelength [Å]	6971.9 ± 1.4
FWHM [km s^{-1}]	1004 ± 168
Flux density (6716 Å)*	1.11 ± 0.48
Flux density (6731 Å)*	2.60 ± 0.64
Flux ratio (6716/6731)	0.43 ± 0.21
Gas density [cm^{-3}]	>3000
Narrow Hα flux [erg s^{-1} cm^{-2} lens^{-1}]	$(5.0 \pm 1.5) \times 10^{-17}$

*Peak intensity in units of 10^{-18} erg s^{-1} cm^{-2} Å^{-1} lens^{-1}.

10^4 cm^{-3} (Osterbrock & Ferland 2006), if all (or almost all) the He are He$^+$ ions.

Solving its origin is beyond the scope of this study. This component, together with the broad Hα wing, could influence measurement of the outflowing gas. In the next subsection, we thus preferentially use the spectra at the lenslets far from the center (indicated by black circles in the bottom left panel of figure 1).

4.4 Velocity and density of the outflowing gas

To derive the velocity and the density of the outflowing gas, we used the mean spectrum of the eight lenslets where the excess flux was large and the contamination of the broad line small. If we fitted the spectrum with a single velocity component for narrow lines, the clear blue tail in the [S II] emission remains (upper panels of figure 2). Moreover, the flux ratio of the [S II] emission lines is 1.7, exceeding the allowed range (0.44–1.45; e.g., Sanders et al. 2016). These issues indicate that the fit is not appropriate.

Therefore, we fitted the mean spectrum with an additional velocity component for narrow emission lines (Hα, [N II], and [S II]). Similar to the preexisting narrow line component, the width and the velocity were also tied within this second component. Here, we also added a component at ∼6930 Å, for which the wavelength and the Gaussian width were fixed at the lenslet with the strongest 6925–6940 Å excess flux (shown in yellow in the bottom right panel of figure 1). As a result (table 1), the blue tail is well described by the second narrow component (lower panels of figure 2). This component is about 810 km s^{-1} blueshifted from the brighter component at these lenslets, which is relatively blueshifted with respect to the whole FoV (middle left panel of figure 1). Since the systemic velocity of this object in the literature varies by hundreds of km s^{-1}, we here define the systemic velocity as the mean velocity of the narrow lines at the north-east and west sides $\gtrsim 1''$ from the center. The blueshift velocity of the outflowing component relative to the systemic velocity is about 860 km s^{-1}, fast enough compared with the escape velocity at NLRs (∼500 km s^{-1}).

If the gas density is low ($\lesssim 100$ cm^{-3}), the [S II] flux ratio (6717 Å/6731 Å) is about 1.4–1.45. When the density exceeds $\sim 10^{3.5}$ cm^{-3}, the [S II] flux ratio becomes ∼0.44–0.5 (e.g., Sanders et al. 2016). With the two-component fit, we estimate that the brighter component has a density of about 300 cm^{-3}, similar to the typical density in NLRs of AGNs. On the other hand, the outflowing component is very dense, >3000 cm^{-3}.

Albeit with large uncertainties, the [N II]λ6583/Hα and [S II]λ6716 + λ6731/Hα flux ratios of the outflowing component (2.4 ± 0.8 and 1.8 ± 0.6, respectively) indicate a non-stellar origin for its ionization (e.g., Kewley et al. 2006).

Assuming Case B recombination at 10^4 K with solar abundance, the ionized gas mass $M_{\rm gas}$ is in principle estimated from the Hα luminosity $L_{\rm H\alpha}$ and the electron density n as $M_{\rm gas} \approx 3.3 \times 10^8\, M_\odot\, (L_{\rm H\alpha}/10^{43}\,[{\rm erg\,s^{-1}}])\, (n/100\,[{\rm cm^{-3}}])^{-1}$ (Carniani et al. 2015; Nesvadba et al. 2017). Since the gas density affects the estimation of the gas mass inversely, a conventional assumption for the density of ∼100 cm^{-3} must have led to overestimations in the gas mass, the outflow rate, the kinetic power injection, etc. for the feedback process. The flux of the Hα narrow line of the outflowing component is quite uncertain, since it is veiled by the strong broad line. Taking the fitting results at face value, and assuming that the eight lenslets contain 10% of the total (all 27 lenslets plus surrounding lenslets leaked via image smearing) flux of the Hα narrow line in the outflowing gas, we estimate the outflowing gas mass to be $<1.6 \times 10^4\, M_\odot$. Given that the radial extension of the outflowing region is much smaller than the PSF FWHM (0.″37), we presume that it is 0.1 × 0.″37 (i.e., 29 pc). Assuming that the line-of-sight velocity (860 km s^{-1}) is cos 45° (subsection 4.3) times the outflow velocity $V_{\rm out}$ (i.e., 1200 km s^{-1}), this region is likely to have been launched from the center 0.13 Myr ago for a duration of 2.3×10^4 yr (i.e., 29 pc/1200 km s^{-1}; $t_{\rm out}$). Then, the gas outflow rate, $M_{\rm gas}/t_{\rm out}$, is estimated to be $<0.7\, M_\odot$ yr^{-1} (∼90% of the current gas accretion rate; section 2).

Similarly, the kinetic power $M_{\rm out}(V_{\rm out}^2 + 3\sigma^2)/2$ and the momentum $M_{\rm out} V_{\rm out}$ contained in the outflowing gas

lead to estimates for the kinetic energy injection rate ($<4.4 \times 10^{41}\,\mathrm{erg\,s^{-1}}$) and the momentum flux ($<5.3 \times 10^{33}\,\mathrm{g\,cm\,s^{-1}}$), where σ is the line-of-sight velocity dispersion of the blueshifted line. The ratio of the kinetic energy injection rate to the bolometric luminosity is low ($\lesssim 0.07\%$), similar to high-z AGNs (Kakkad et al. 2016). The momentum flux is comparable to the radiation momentum L_{bol}/c received by the outflowing region with a solid angle subtended at the nucleus of $2\pi(1 - \cos 50^{\circ}) = 0.18 \times 4\pi$), where c is the speed of light.

5 Summary and discussions

We observed the nearest ($z = 0.039$) AGN with prominent blueshift/tail in [O III] emission from a sample of such objects collected from the literature, to examine the putative AGN feedback process on its host galaxy, by utilizing the unique capability of Subaru, optical IFU with AO assistance (Kyoto 3D II with AO188). The optical waveband enabled us to observe the density-sensitive [S II] doublets, with which we could measure the gas density via the flux ratio. Through spectral fitting for the 615 lenslets, over 3.″1 (2.4 kpc) of IRAS 04576+0912, we obtained the kpc-scale structures in velocity, flux, and ionization sources. Many lenslets turned out to exhibit a blue tail in the [S II] emission. Through the location and the distribution of the lenslets with high excess flux at the corresponding wavelengths, and fitting results for their mean spectrum, we found a fast ($\sim$860 km s^{-1} blueshift), dense ($>3000\,\mathrm{cm^{-3}}$), wide-angle (with a half-opening angle of $\sim 50^{\circ}$), and offset outflow at 100 pc scales. In short, a gas outflow with a rate of $\lesssim 90\%$ of the accretion rate was launched 0.13 Myr ago (over 2.3×10^4 yr). The large opening angle and the high gas outflow-to-accretion ratio may favor the AGN feedback hypothesis, although the outflow seems to be neither spherical nor continuous. The inferred kinetic power injection rate ($\lesssim 0.07\%$ of L_{bol}) of this ionized gas outflow seems insufficient to influence the whole host galaxy. A conventional assumption of a low gas density, $\sim 100\,\mathrm{cm^{-3}}$, must have overestimated the feedback process.

Outflow launched by AGNs with high accretion rates may be commonly fast and dense. AO-assisted NIR IFU observations of NGC 1068, which is a type-2 analogue of NLS1s (Kawaguchi 2003), reveal the outflow kinematics in the central 100 pc-scales (Müller-Sánchez et al. 2011). Ozaki (2009) showed that the outflowing clumps (with gas densities of $\sim 10^5\,\mathrm{cm^{-3}}$) with a variety of column densities are likely accelerated by radiation from the center.

We leave further analysis, including maps for other line ratios and the narrow-line width (as a tracer for ISM disturbance), as well as the decomposition between the galactic rotation and the NLR outflow, for the next paper. Three-dimensional kinematical modeling to reproduce these maps will follow.

Acknowledgments

This work is based on data collected at the Subaru Telescope, which is operated by the National Astronomical Observatory of Japan. We are grateful to the staff of the Subaru Telescope, and the anonymous referee, Masayuki Akiyama, and Xiaoyang Chen for helpful comments. TK is supported by JSPS KAKENHI (17K05389).

References

Aoki, K., Kawaguchi, T., & Ohta, K. 2005, ApJ, 618, 601
Balmaverde, B., et al. 2016, A&A, 585, A148
Barbosa, F. K. B., Storchi-Bergmann, T., Cid Fernandes, R., Winge, C., & Schmitt, H. 2009, MNRAS, 396, 2
Boroson, T. 2005, AJ, 130, 381
Carniani, S., et al. 2015, A&A, 580, A102
Carniani, S., et al. 2016, A&A, 591, A28
Cresci, G., et al. 2015, A&A, 582, A63
Di Matteo, T., Springel, V., & Hernquist, L. 2005, Nature, 433, 604
Gabor, J. M., & Bournaud, F. 2014, MNRAS, 441, 1615
Husemann, B., Scharwächter, J., Bennert, V. N., Mainieri, V., Woo, J.-H., & Kakkad, D. 2016, A&A, 594, A44
Kakkad, D., et al. 2016, A&A, 592, A148
Kauffmann, G., et al. 2003, MNRAS, 346, 1055
Kawaguchi, T. 2003, ApJ, 593, 69
Kawaguchi, T., Aoki, K., Ohta, K., & Collin, S. 2004, A&A, 420, L23
Kewley, L. J., Groves, B., Kauffmann, G., & Heckman, T. 2006, MNRAS, 372, 961
Komossa, S., Xu, D., Zhou, H., Storchi-Bergmann, T., & Binette, L. 2008, ApJ, 680, 926
Lena, D., et al. 2015, ApJ, 806, 84
Marziani, P., Zamanov, R. K., Sulentic, J. W., & Calvani, M. 2003, MNRAS, 345, 1133
Matsubayashi, K., Sugai, H., Shimono, A., Akita, A., Hattori, T., Hayano, Y., Minowa, Y., & Takeyama, N. 2016, PASP, 128, 095003
Mazzalay, X., Rodríguez-Ardila, A., Komossa, S., & McGregor, P. J. 2013, MNRAS, 430, 2411
Mitsuda, K., et al. 2016, Proc. SPIE, 9908, 99082M
Müller-Sánchez, F., Prieto, M. A., Hicks, E. K. S., Vives-Arias, H., Davies, R. I., Malkan, M., Tacconi, L. J., & Genzel, R. 2011, ApJ, 739, 69
Nesvadba, N. P. H., De Breuck, C., Lehnert, M. D., Best, P. N., & Collet, C. 2017, A&A, 599, A123
Ohta, K., Aoki, K., Kawaguchi, T., & Kiuchi, G. 2007, ApJS, 169, 1
Osterbrock, D. E., & Ferland, G. J. 2006, Astrophysics of Gaseous Nebulae and Active Galactic Nuclei, 2nd ed. (Sausalito, CA: University Science Books)
Ozaki, S. 2009, PASJ, 61, 259
Sanders, R. L., et al. 2016, ApJ, 816, 23
Schawinski, K., Thomas, D., Sarzi, M., Maraston, C., Kaviraj, S., Joo, S.-J., Yi, S. K., & Silk, J. 2007, MNRAS, 382, 1415
Silk, J., & Rees, M. J. 1998, A&A, 331, L1

Storchi-Bergmann, T., McGregor, P. J., Riffel, R. A., Simões Lopes, R., Beck, T., & Dopita, M. 2009, MNRAS, 394, 1148
Sugai, H., et al. 2010, PASP, 122, 103
Sulentic, J. W., Bachev, R., Marziani, P., Negrete, C. A., & Dultzin, D. 2007, ApJ, 666, 757
van Dokkum, P. G. 2001, PASP, 113, 1420
Véron-Cetty, M.-P., Véron, P., & Gonçalves, A. C. 2001, A&A, 372, 730
Villar-Martín, M., Arribas, S., Emonts, B., Humphrey, A., Tadhunter, C., Bessiere, P., Cabrera Lavers, A., & Ramos Almeida, C. 2016, MNRAS, 460, 130
Vogt, F. P. A., et al. 2017, Phys. Rev. X, 7, 021044
Wyithe, J. S. B., & Loeb, A. 2003, ApJ, 595, 614
Zamanov, R., Marziani, P., Sulentic, J. W., Calvani, M., Dultzin-Hacyan, D., & Bachev, R. 2002, ApJ, 576, L9